

Article

# Schwertmannite Adherence to the Reactor Wall during the Bio-Synthesis Process and Deterioration of Its Structural Characteristics and Arsenic(III) Removal Efficiency

Jian Zhang <sup>1,†</sup>, Jing Shi <sup>2,†</sup>, Shasha Zhang <sup>3</sup>, Lixiang Zhou <sup>4</sup>, Jianmin Xu <sup>1</sup>, Yuanying Ge <sup>1</sup>,  
Wenhua Fan <sup>1</sup> and Fenwu Liu <sup>1,\*</sup>

<sup>1</sup> Environmental Engineering Laboratory, College of Resource and Environment, Shanxi Agricultural University, Taigu 030801, China; zhangjian82@sxau.edu.cn (J.Z.); xujianmin@sxau.edu.cn (J.X.); sxaugyy@sxau.edu.cn (Y.G.); fanwh@sxau.edu.cn (W.F.)

<sup>2</sup> Analytical Instrumentation center, Institute of coal chemistry, Chinese Academy of Sciences, 27 South Taoyuan Road, Taiyuan 030001, China; shijing@sxicc.ac.cn

<sup>3</sup> School of Environmental Science and Engineering, Shandong University, Jinan 250100, China; sdzss@mail.sdu.edu.cn

<sup>4</sup> Department of Environmental Engineering, College of Resources and Environmental Sciences, Nanjing Agricultural University, Nanjing 210095, China; lxzhou@njau.edu.cn

\* Correspondence: liufenwu@sxau.edu.cn; Tel.: +86-354-628-8322

† These authors contributed equally to this work.

Academic Editor: Karen Hudson-Edwards

Received: 27 March 2017; Accepted: 19 April 2017; Published: 22 April 2017

**Abstract:** Schwertmannite, a kind of iron oxyhydrogensulfate mineral, can removal arsenic(III) from arsenic(III)-bearing groundwater by the adsorption process. In this study, schwertmannite was bio-synthesized by *Acidithiobacillus ferrooxidans* LX5 in shaking flasks (160 rpm) containing a 0.16 mol/L FeSO<sub>4</sub> liquid solution. After bio-synthesis, 25.5% of the bio-synthesized schwertmannite adhered to the reactor wall (designated as adhered-sch) and the remainder was suspended in the system (designated as suspended-sch). Particles of adhered-sch exhibited a fractured structure with a small specific surface area (4.36 m<sup>2</sup>/g) and total pore volume (3.13 × 10<sup>-2</sup> cm<sup>3</sup>/g). In contrast, suspended-sch had a spiny structure (similar in appearance to a hedgehog), and a larger specific surface area (9.62 m<sup>2</sup>/g) and total pore volume (8.01 × 10<sup>-2</sup> cm<sup>3</sup>/g). When 0.25 g/L of adhered-sch was used as an adsorbent for arsenic(III) removal from 1 mg/L arsenic(III)-bearing waters (at pH 7.5), the arsenic(III) removal efficiency was 43.2% after 4 h of adsorption. However, this efficiency could be increased by 50% by using suspended-sch as the adsorbent. Furthermore, by adding 13.3 g/L and 26.7 g/L additional schwertmannite into the reactor system prior to schwertmannite bio-synthesis, all synthesized schwertmannite remained suspended in the bio-synthesis systems, and the ferrous ions' bio-oxidation efficiency was improved to a certain extent. Due to the friction effect between the introduced schwertmannite and the reactor wall, adhered-sch was eliminated. The outcomes of this study will provide the necessary data for schwertmannite bio-synthesis and arsenic(III) removal from arsenic(III)-bearing groundwater.

**Keywords:** adhered schwertmannite; suspended schwertmannite; specific surface area; arsenic(III); adsorption

## 1. Introduction

Arsenic is defined as a Category 1 and Group A human carcinogen by the International Association for Research on Cancer because of its high toxicity and carcinogenicity [1,2]. The predominant forms of arsenic are commonly present in two valence states as inorganic species arsenic(III) and arsenic(V), with the former being more poisonous than the latter [3]. In many cases, groundwater is frequently contaminated by arsenic due to natural geological processes and many anthropogenic activities [4], and arsenic(III) is the predominant arsenic species existing in anoxic groundwater [5]. High health risks caused by drinking high-arsenic groundwater is a significant problem in many parts of the world, including China [6]. In China, high arsenic-bearing groundwater mainly exists in Inner Mongolia, Shanxi, Xinjiang, etc., including 40 counties of eight provinces. For example, arsenic concentration in groundwater samples collected from the Hetao Plain in the Inner Mongolia Autonomous Region, Datong in Shanxi province, and Dzungaria district in Xinjiang province can be up to 1.09 mg/L [7], 1.82 mg/L [8], and 0.85 mg/L [9], respectively. It is obvious that the highest concentration of arsenic in arsenic-bearing groundwater in different regions in China can reach, or exceed, 1 mg/L. Except for China, the arsenic levels in groundwater from many other countries in the world often surpass 1 mg/L [10,11]. For example, 17 out of 52 districts of Bangladesh had a maximum level of arsenic in groundwater exceeding 1 mg/L [11]. Thus, it is highly desirable to develop approaches that can significantly remove arsenic(III) from arsenic-bearing groundwater and improve the quality of groundwater resources.

Numerous technologies have been presented for treating arsenic(III)-bearing water, such as membrane filtration [12], ion exchange [13], and electrolysis [14]. However, high cost, lack of selectivity, and poor performance restricts the practical application of these methods to a certain extent. Adsorption technology is an adopted technique for arsenic(III) removal from arsenic(III)-bearing water due to its easy operation, high capacity, fast kinetic reactions, and mild regeneration condition [15–17]. Schwertmannite, an amorphous iron oxyhydroxysulfate mineral, is commonly synthesized in an iron sulfate-rich acidic environment, has proved to be a good scavenger of arsenic(III) [18–20]. Liao et al. [21] observed that arsenic(III) adsorption by schwertmannite improves with the increase of the solution pH in the range of 3–9 and the maximum removal efficiency of arsenic(III) occurs at solution pH 7–9. It is indicated that using schwertmannite as an adsorbent shows the great potential application in arsenic(III) removal from arsenic(III)-bearing groundwater because the pH of groundwater is often in the range of 6.5–9.0 [22,23]. The mechanism of arsenic(III) adsorption on schwertmannite involves either ligand exchange between arsenic(III) species and a hydroxyl group and sulfate [21], or the formation of arsenic(III)-Fe(III)-SO<sub>4</sub><sup>2-</sup> precipitates [24] on the schwertmannite surface. Paikaray et al. [24] found that an amount of SO<sub>4</sub><sup>2-</sup> can be released from schwertmannite into the solution during arsenic(III) adsorption. Therefore, schwertmannite, with a large specific surface area, exhibited a high removal efficiency for arsenic(III) from groundwaters [20,25].

Schwertmannite can be synthesized by biogenic oxidation of FeSO<sub>4</sub> by *Acidithiobacillus ferrooxidans* (*A. ferrooxidans*) followed by subsequent ferric ion hydrolysis [21,26]. FeSO<sub>4</sub> bio-oxidation by *A. ferrooxidans* is an attractive technology for schwertmannite production because the reaction time is less than 72 h and the reaction can be carried out at room temperature (20–30 °C). However, some bio-schwertmannite is adhered to the reactor wall (adhered-sch), while the rest of the bio-schwertmannite is suspended in the system (suspended-sch) during schwertmannite bio-synthesis by *A. ferrooxidans* when the hydraulic shear force in the schwertmannite bio-synthesis system is relatively weak. This adhesion phenomenon can cause certain problems for schwertmannite collection from a bio-reactor, but not enough attention has been given to it in previous studies. Moreover, the characteristic difference between adsorbed-sch and suspended-sch has not been reported.

This study was designed to (1) investigate the difference in structural characteristics, specific surface area, total pore volume, and arsenic(III) removal efficiency between adsorbed-sch and suspended-sch; and (2) examine the removal of adhered-sch from the bio-synthesis reactor wall by introducing additional schwertmannite prior to schwertmannite bio-synthesis.

## 2. Materials and Methods

Analytical grade reagents and chemicals were used for all the experiments. All solutions were prepared with deionized water immediately before use.

### 2.1. Preparation of *A. ferrooxidans* Cell Suspensions

The acidophilic chemoautotrophic bacterium *A. ferrooxidans* LX5 (CGMCC No. 0727) was obtained from the China General Microbiological Culture Collection Center (Beijing, China). Modified 9 K liquid medium [27] was used to culture *A. ferrooxidans* LX5. The pH of the liquid medium was then adjusted to pH 2.50 with sulfuric acid. The *A. ferrooxidans* LX5 was cultured in a rotary shaker (SHZ-82, Jintan city jieruier electric Co., Ltd., Jintan, China) at 28 °C and 180 rpm until the ferrous ions were completely bio-oxidized. After *A. ferrooxidans* LX5 culturing, the microbial density of the cultures was determined using the plate count method to be  $3 \times 10^7$  cells/mL. The cultures were filtered through quantitative filter paper to remove iron-based precipitate, and then the filtrates were centrifuged using a high-speed centrifuge (Neofuge 23 R, Shanghai Lishen Scientific Equipment Co., Ltd., Shanghai, China) at 12,000 rpm for 15 min at 4 °C [28] to settle the *A. ferrooxidans* LX5 cells in the bottom of the centrifugation tube. The cells were washed twice with sulfuric acid and centrifuged again, after which the cells were re-suspended in pH 2.50 sulfuric acid. The volume ratio between filtrates and sulfuric acid used to suspend the *A. ferrooxidans* LX5 cells was 15:1. In other words, the bacterial density in *A. ferrooxidans* LX5 cell suspensions was  $4.5 \times 10^8$  cells/mL. The *A. ferrooxidans* LX5 cell suspensions, which contained no ferric ions, were used in further studies.

### 2.2. Preparation of Additional Schwertmannite in a 25 L Bioreactor

Schwertmannite was obtained using *A. ferrooxidans* LX5 to bio-oxidize the ferrous ion solution. Ferrous ion oxidation by *A. ferrooxidans* LX5 cells was carried out in 15 L of solution containing 0.16 mol/L ferrous ions (added as  $\text{FeSO}_4 \cdot 7\text{H}_2\text{O}$ ), which was dispensed into a 25 L bioreactor fitted with an air compressor and temperature control device. The aeration rate and temperature were maintained at 0.055 m<sup>3</sup>/min and 28 °C, respectively. A 100 mL quantity of *A. ferrooxidans* LX5 cell suspension was added into the bio-reactor. After 72 h, the ferrous ions were completely bio-oxidized. Then, the cultures were filtered through quantitative filter paper to harvest the suspended iron-based precipitate. The precipitate was collected after washing it twice with distilled water. The rinsed precipitate was then dried at 55 °C to constant weight, passed through a 100 mesh screen, and characterized using X-ray diffraction (XRD) and field-emission scanning electron microscopy (SEM) technologies. The results of XRD and SEM of the rinsed precipitate certified that the collected precipitate was schwertmannite.

### 2.3. Schwertmannite Bio-Synthesis Experiment Introducing Additional Schwertmannite before Bio-Synthesis

The schwertmannite bio-synthesis experiments were carried out in 150 volumes of solution containing 0.16 mol/L ferrous ions (added as  $\text{FeSO}_4 \cdot 7\text{H}_2\text{O}$ ) and dispensed into 250 mL glass Erlenmeyer flasks. A 1 mL cell suspension of *A. ferrooxidans* LX5 was added to each Erlenmeyer flask. Then, either 0 g, 2 g, or 4 g of additional schwertmannite was added into each flask to yield concentrations of 0 g/L (CK treatment), 13.3 g/L, and 26.7 g/L, respectively. CK treatments was conducted in nine replicates, and other treatments were performed in triplicate. The initial pH of all systems was adjusted to pH 2.50 by adding 1 mol/L  $\text{H}_2\text{SO}_4$  or NaOH. The systems were incubated at 28 °C while flasks were shaken at 160 rpm. During incubation, the pH in the systems was monitored. At 12 h intervals 0.5 mL of solution was withdrawn from each flask, filtered through a 0.22 µm membrane filter, and analyzed to determine ferrous ions' bio-oxidation efficiency. After 60 h, the ferrous ions were nearly completely bio-oxidized (ferrous ion bio-oxidation efficiency above 99%) in all treatments. Then the solution in each flask was filtered, the schwertmannite washed twice with distilled water, and dried at 55 °C to constant weight. In the CK treatment, some amount of schwertmannite was observed to have adhered on the flask wall, while some

remained suspended in the solution. The suspended schwertmannite was collected by filtration as just described, and the adhered schwertmannite was removed from the flask wall by manual force using a glass rod. The adhered and suspended schwertmannite were weighed separately, passed through a 100 mesh screen, and analyzed to determine the specific surface area, total pore volume, and pore size distribution. Samples were also examined using XRD and SEM. The schwertmannite biosynthesis pathway is shown in Figure 1.

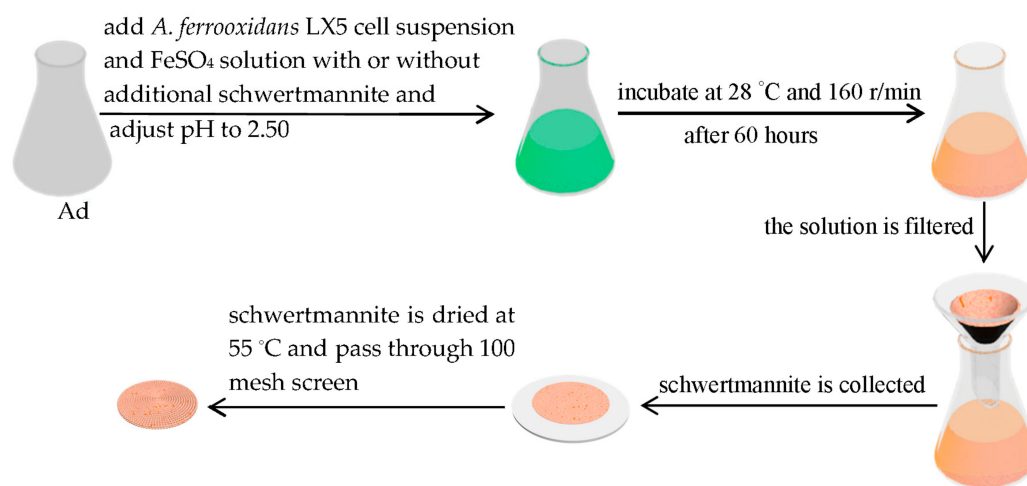


**Figure 1.** The schwertmannite biosynthesis pathway.

#### 2.4. Effect of Adhered, Suspended-Schwertmannite on Arsenic(III) Adsorption

A 1000 mg/L arsenic(III) stock solution was prepared by dissolving 0.6595 g of the dried  $\text{As}_2\text{O}_3$  in 20 mL of 40% NaOH solution; the mixture then was transferred to a 500 mL volumetric flask and the volume was completed with deionized water. The arsenic(III) stock solution was stored at 4 °C before use. Before each experiment, a solution with 1 mg/L arsenic(III) concentration was prepared by diluting the stock solution. The solution was adjusted to pH 7.50 by adding HCl or NaOH, drop-wise. Then, 40 mL of 1 mg/L arsenic(III) solution was placed in 100-mL capped plastic bottles (inner diameter 46 mm), and amended with either 0 g of schwertmannite (CK, treatment 1), 0.010 g of adhered-schwertmannite (treatment 2), or 0.010 g of suspended-schwertmannite (treatment 3). Each treatment was prepared in triplicate. All systems were shaken in a rotary shaker at 28 °C and 160 rpm for 4 h. Liao et al. [21] found that 4 h is enough time for arsenic(III) to adsorb in bio-schwertmannite and the bio-schwertmannite exhibits no mineralogy phase change under these adsorption conditions. After shaking for 4 h, the samples in different systems were filtered through a 0.45  $\mu\text{m}$  membrane and determined for arsenic(III). Then the arsenic(III) removal efficiency was calculated according to the following formula:

$$\text{The arsenic(III) removal efficiency} = \left[ \frac{C_{\text{arsenic(III)}}}{\text{total arsenic(III) concentration}} \right] \times 100\%$$

where  $C_{\text{arsenic(III)}}$  is the arsenic(III) concentration in the filtrate collected after 4 h of shaking.

#### 2.5. Analytical Procedures

Solution pH was determined using a pH meter (pHS-3C, Shanghai Yueping Scientific Instruments Co., Ltd., Shanghai, China) with a resolution of 0.01. The 1,10-phenanthroline method was used to analyze ferrous ion concentration. The ferrous ions' bio-oxidation efficiency was calculated based on the difference between the initial ferrous ions and the ferrous ion concentration at different sampling times [27]. The weight of solid precipitates was measured using an electronic balance (BS 124S, Beijing

Sartorius Instrument Co., Beijing, China) with a precision of 0.0001 g. The mineral morphology or phase of precipitates was determined through field-emission scanning electron microscopy (SEM, JSM-7001F, JEOL, Tokyo, Japan) or power X-ray diffraction (XRD, MiniFlex II, Rigaku, Tokyo, Japan) [29]. Total pore volume was determined using a surface area and porosimetry analyzer (Quantachrome, Boynton Beach, FL, USA). The specific surface area of minerals was determined using the same porosimetry analyzer with the multi-point Brunauer–Emmett–Teller (BET) method, and the Barrett–Joyner–Halenda (BJH) pore size distribution was calculated from the adsorption isotherm [30,31]. Within the arsenic(III) removal systems in this study, there were no other arsenic forms existing in the arsenic(III)-bearing solution, just arsenic(III). Therefore, the arsenic(III) concentration was equal to the total arsenic concentration in arsenic(III)-bearing solutions used here. Arsenic(III) concentration, or total arsenic concentration, in solution was analyzed through a dual-channel atomic fluorescence photometer (AFS-2100, Beijing Haiguang Instrument Co., Ltd., Beijing, China) [32] with a detection limit of 0.01  $\mu\text{g/L}$ .

### 3. Results and Discussion

#### 3.1. Schwertmannite Bio-Synthesized in 25 L Bioreactor

The scanning electron microscopy (SEM) images and X-ray diffraction (XRD) patterns of schwertmannite bio-synthesized in the 25-L bio-reactor are illustrated in Figure 2. No single, sharp, intense, and well-recognizable peaks could be observed on the XRD patterns (Figure 1a), indicating that the mineral harvested from the reactor is an amorphous body consistent with the schwertmannite feature. In addition, the mineral harvested from the bio-reactor has the obvious characteristic peaks at  $2\theta = 26.32^\circ$ ,  $35.12^\circ$ ,  $55.32^\circ$ , and  $63.74^\circ$ . In addition, Figure 2b confirms that an amorphous mineral was the sole mineral phase detectable in the synthesized product. According to PDF 47-1775 [33] and the results of XRD and SEM investigated here, schwertmannite is the only mineral synthesized in this system that has a typical spiny spheroidal structure similar in appearance to a hedgehog. This structure of schwertmannite has also been reported in previous studies [20,21].

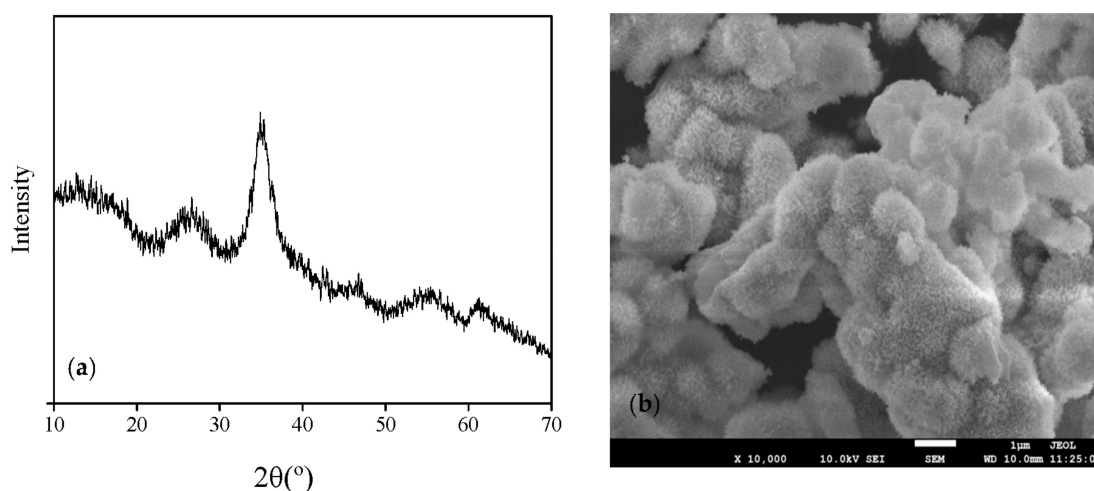


**Figure 2.** (a) X-ray diffraction patterns and (b) scanning electron microscopy images of schwertmannite bio-synthesized in a 25-L bio-reactor.

#### 3.2. The pH and Ferrous Ions' Efficiency Variations during Schwertmannite Bio-Synthesis with the Introduction of Additional Schwertmannite

The variations in pH and ferrous ion bio-oxidation efficiency that occurred during schwertmannite bio-synthesis when additional schwertmannite was introduced into the reactors are shown in Figure 3. As shown, the pH slightly increased, initially, from 2.50 to 2.55–2.58 regardless of the addition of

schwertmannite (Figure 3a). During 12–60 h, pH in all treatments significantly decreased, but the rate of pH decline in the treatment with 13.3 g/L of added schwertmannite was relatively rapid than in the CK treatment (no added schwertmannite). For example, after 60 h, the pH in CK treatment was 2.21, while that in the treatment consisting of an added 13.3 g/L of schwertmannite was 2.16. However, when the amount of added schwertmannite was 26.7 g/L, the pH decreased more slowly than in the treatment consisting of 13.3 g/L of added schwertmannite, reaching 2.19 after 60 h incubation. The pH changes in different treatments were governed by ferrous ion oxidation and ferric ion hydrolysis processes [20,34]. Ferrous ion bio-oxidation efficiency in the presence of added schwertmannite increased sharply during 0–36 h and, thereafter, increased gradually to 100% at 60 h in the CK treatment (Figure 2b). However, the addition of either 13.3 g/L or 26.7 g/L schwertmannite enhanced the ferrous ion bio-oxidation efficiency beyond that achieved in the CK treatment over a short duration. For instance, the ferrous ion bio-oxidation efficiency was 40.2% in the CK treatment after 24 h, but 53.5% and 46.3% in treatments with 13.3 g/L and 26.7 g/L of added schwertmannite, respectively. It is interesting that the ferrous ion bio-oxidation efficiency in the treatment that added 13.3 g/L of schwertmannite increased quicker than in the treatment that added 26.7 g/L of schwertmannite. The data in Figure 3a,b lead to the conclusion that a lower pH promotes higher ferrous ion bio-oxidation efficiency or ferric ion hydrolysis efficiency than does a high pH. Therefore, both the pH and the ferrous ion bio-oxidation efficiency can be used as indicators for *A. ferrooxidans* activity during schwertmannite bio-synthesis. It is interesting that in the CK treatment (no added schwertmannite prior to bio-synthesis), 25.5% of the weight of bio-synthesized schwertmannite adhered to the flask walls (designated as adhered-sch), leaving 74.5% suspended in the reactor system (designated as suspended-sch). However, due to the friction effect between the added schwertmannite and the reactor wall, all synthesized schwertmannite remained suspended in systems to which an additional 13.3 g/L or 26.7 g/L schwertmannite was introduced prior to bio-synthesis. Previous research showed that the *A. ferrooxidans* cells can be covered with, or absorbed by, iron oxyhydroxysulfate minerals during iron oxyhydroxysulfate minerals bio-synthesis by *A. ferrooxidans* [35,36]. Adhered-sch formation caused a large quantity of *A. ferrooxidans* cells to be fixed onto the flask wall, thereby removing them from the liquid phase in the reactor system. Hence, the ferrous ion bio-oxidation efficiency in the CK treatment was lower than in treatments consisting of 13.3 g/L and 26.7 g/L of added schwertmannite. Compared with the systems containing 13.3 g/L or 26.7 g/L added schwertmannite, the pH in the CK treatment was relatively higher because the ferric ion hydrolysis process was weakened under the lower ferrous ion bio-oxidation conditions. Furthermore, ferrous ion bio-oxidation was obviously inhibited when the amount of added schwertmannite increased from 13.3 g/L to 26.7 g/L. In other words, when too much schwertmannite was introduced into a bio-synthesis system, some *A. ferrooxidans* cells were absorbed on the schwertmannite surface [37], thus decreasing the ferrous ion bio-oxidation efficiency (by reduced mass transfer between *A. ferrooxidans* cells and oxygen, ferrous ions, carbon dioxide, and other environmental components). Nevertheless, there was no significant difference in the net weight of newly-bio-synthesized schwertmannite (4.20–4.28 g/L) among the treatments.

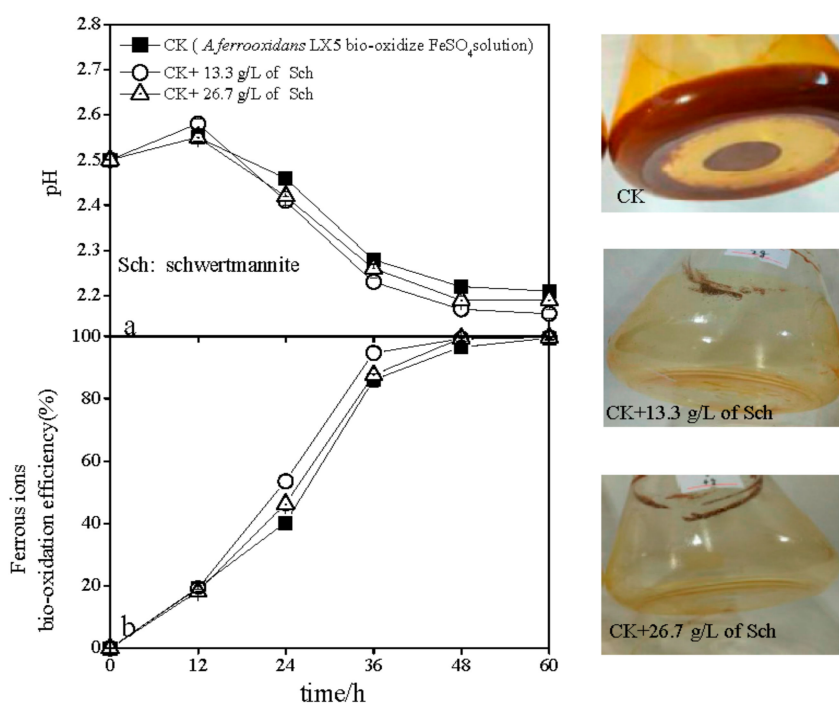


**Figure 3.** Changes in pH (a) and ferrous ion bio-oxidation efficiency (b) during schwertmannite bio-synthesis without (CK) and with additional schwertmannite. Photographs are of the actual flasks used in different treatments taken at the conclusion of schwertmannite bio-synthesis.

### 3.3. The Structural Characteristics of Adhered-Sch and Suspended-Sch

The X-ray diffraction patterns, scanning electron microscopy images, and specific surface area of adhered-sch and suspended-sch collected from the CK treatments are shown in Figure 4. As in the X-ray diffraction patterns (XRD) shown in Figure 1a, it is obvious that the mineral phase of both adhered-sch and suspended-sch was indeed schwertmannite (Figure 4a,b). The color of schwertmannite was ochre-yellow. Figure 3c,d show the difference that existed in the morphology of adhered-sch and suspended-sch. The suspended-sch has an aggregated spiny spheroidal structure that resembles that of a hedgehog and a particle size of approximately 1  $\mu\text{m}$  (Figure 4c), and was similar to the structure of suspended schwertmannite collected from the 25 L bio-reactor (Figure 2b). However, the structure of adhered-sch was smooth and spheroidal, and approximately 4  $\mu\text{m}$  in diameter, with many cracks embedded in the particles (Figure 4d). In fact, bio-synthesized schwertmannite that had a fractured structure was also observed in a previous study [38], although the reason for this phenomenon was not given. Furthermore, the specific surface areas of adhered-sch and suspended-sch were 4.36  $\text{m}^2/\text{g}$  and 9.62  $\text{m}^2/\text{g}$ , respectively. The suspended-sch in the present study had a relatively low specific surface area compared to that observed by Bigham et al. [39] but was comparable to values recently reported by Liao et al. [28] (3.42–23.45  $\text{m}^2/\text{g}$ ) and Liu et al. [20] (10.66  $\text{m}^2/\text{g}$ ). Overall, the bio-synthesized schwertmannite that adhered to the reactor wall exhibited a significantly different structure with a much smaller specific surface area to that of the spiny spheroidal structure exhibited by bio-synthesized schwertmannite that remained suspended in the reactor system. The spines on the suspended-sch appeared to deteriorate and form larger, smoother particles of adhered-sch.

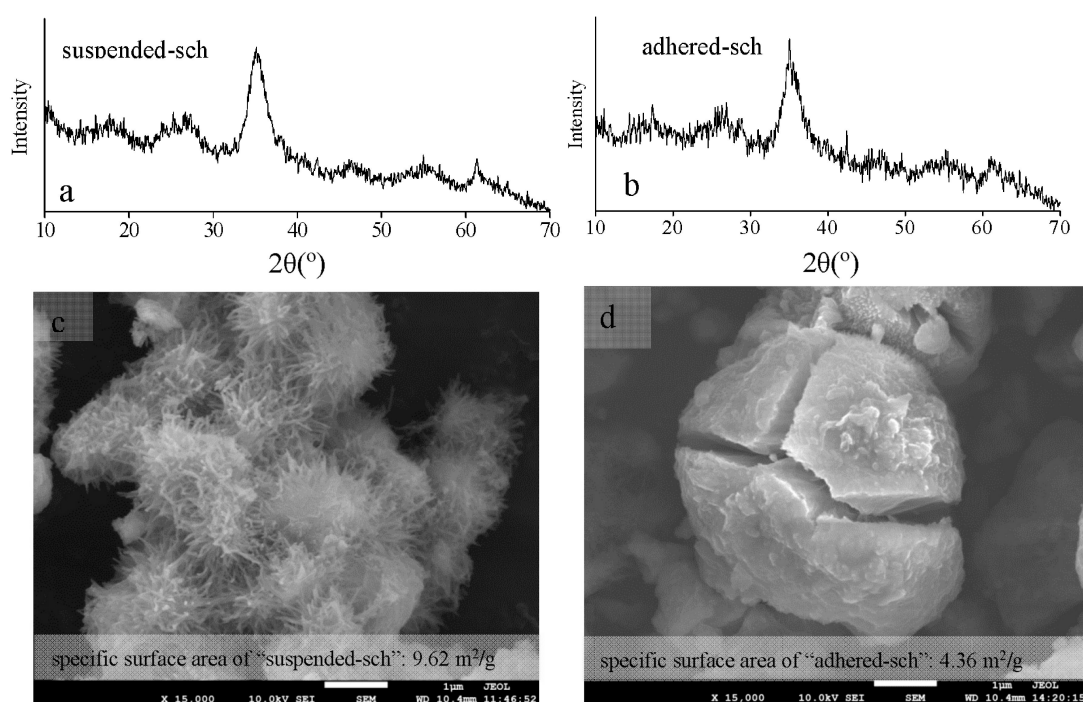


**Figure 4.** X-ray diffraction patterns (a,b); scanning electron microscopy images (c,d); and specific surface area of suspended-sch (a,c) and adhered-sch (b,d).

### 3.4. The Pore Volume and Pore Size Distribution of Adhered-Sch and Suspended-Sch

The surface of schwertmannite particles is porous [14]. A pore system from the perspective of material adsorption is classified into three categories based on pore size: macropore (>50 nm), mesopore (2–50 nm), and micropore (<2 nm) [40,41]. Total pore volume is defined as the sum of micropore, mesopore, and macropore volume [42]. The various types of pore volume of adhered-sch and suspended-sch are shown in Figure 5. The total pore volume of adhered-sch was  $3.13 \times 10^{-2} \text{ cm}^3/\text{g}$ , of which 1.9% was contributed by the micropore volume, 29.4% was contributed by the mesopore volume, and 68.7% was contributed by the macropore volume. The total pore volume of suspended-sch was  $8.01 \times 10^{-2} \text{ cm}^3/\text{g}$ , of which 1.8% was contributed by the micropore volume, 27.4% was contributed by the mesopore volume, and 70.8% was contributed by the macropore volume. In other words, compared with adhered-sch, the total pore volume, micropore volume, mesopore volume, and macropore volume of suspended-sch were increased by 1.56, 1.46, 1.38, and 1.64 times, respectively. The pore volume distributions of adhered-sch and suspended-sch lead to the conclusion that macropores and mesopores occupied approximately 70% and 30%, respectively, of the total pore volume in schwertmannite, and that the micropore volume can be ignored. Dou et al. [18], using  $\text{FeCl}_3$  and  $\text{Na}_2\text{SO}_4$  as reactants, allowed approximately 35 days for schwertmannite chemical synthesis and determined that the specific surface area and the total pore volume of the synthesized schwertmannite reached  $206.1 \text{ m}^2/\text{g}$  and  $2.2 \times 10^{-1} \text{ cm}^3/\text{g}$ , respectively. Results from the present study combined with those from previous studies indicate that the specific surface area of schwertmannite is significantly correlated with the total pore volume. It is worth mentioning that the specific surface area of bio-synthesized schwertmannite is relatively lower than that of schwertmannite chemically synthesized using the  $\text{FeCl}_3$  and  $\text{Na}_2\text{SO}_4$  reaction method [18], but close to that of schwertmannite chemically synthesized through oxidation of  $\text{FeSO}_4$  by  $\text{H}_2\text{O}_2$  (specific surface area of schwertmannite:  $2.06\text{--}16.30 \text{ m}^2/\text{g}$ ) [20]. Regardless of the process used, improving the specific surface area of schwertmannite is another vital task for schwertmannite bio-synthesis during the engineering process.

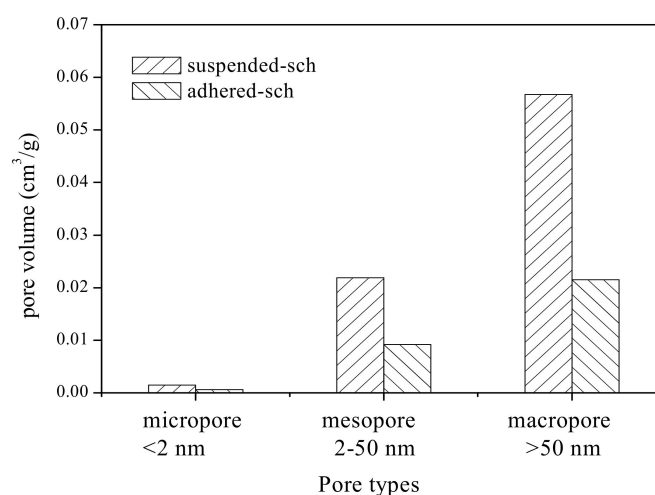


**Figure 5.** Micropore, mesopore, and macropore volumes of schwertmannite adhered to the flask wall during bio-synthesis (adhered-sch) and schwertmannite suspended in the liquid system during bio-synthesis (suspended-sch).

As mentioned earlier, schwertmannite is a potential adsorption material for removing arsenic(III) from wastewater [21–24]. Mesopore distribution has a profound influence on the adsorption capacity of adsorption materials [43]. In the current study, the pore volume attributed to mesopores accounted for 29.4% and 27.3% of total pore volume in adhered-sch and suspended-sch, respectively. However, the specific surface area represented by mesopores accounted for 67.7% and 62.9% of the total specific surface area in adhered-sch and suspended-sch, respectively. The accumulated pore volume and specific surface area for different mesopore sizes in adhered-sch and suspended-sch are presented in Figure 6. The mesopore size in adhered-sch and suspended-sch materials varied from ~3 nm to 30 nm, but was not significantly different in the two materials. Pore volume contributed by pores with diameters ~3–20 nm accounted for 55.1% and 47.6% of total mesopore volume in adhered-sch and suspended-sch, respectively (Figures 5 and 6a). However, the specific surface area from pores with diameters between ~3 nm and 20 nm accounted for 81.4% and 71.9% of the total mesopore-specific surface area in adhered-sch and suspended-sch, respectively (Figure 6b). Thus, although the mesopores in schwertmannite account for only a modest pore volume, these pores (and especially the mesopores of ~3–20 nm diameter) make a significant contribution to the specific surface area of this material.

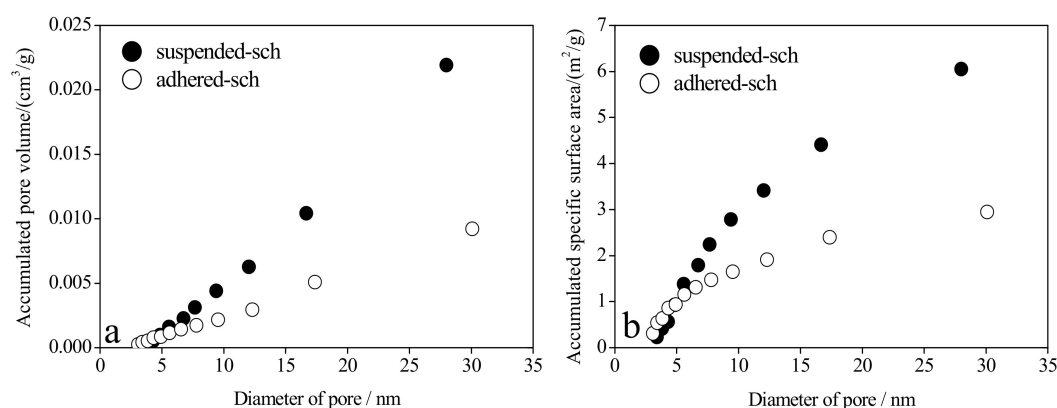


**Figure 6.** Accumulated pore volume (a) and accumulated specific surface area (b) of different mesopore sizes in schwertmannite adhered to the flask wall during bio-synthesis (adhered-sch) and schwertmannite suspended in the liquid system during bio-synthesis (suspended-sch).

### 3.5. Arsenic(III) Removal Efficiency of Adhered-Sch and Suspended-Sch

The arsenic(III) removal efficiency of adhered-sch and suspended-sch is shown in Figure 7. No arsenic(III) removal was obvious when no schwertmannite was added to the arsenic(III)-bearing solution system.

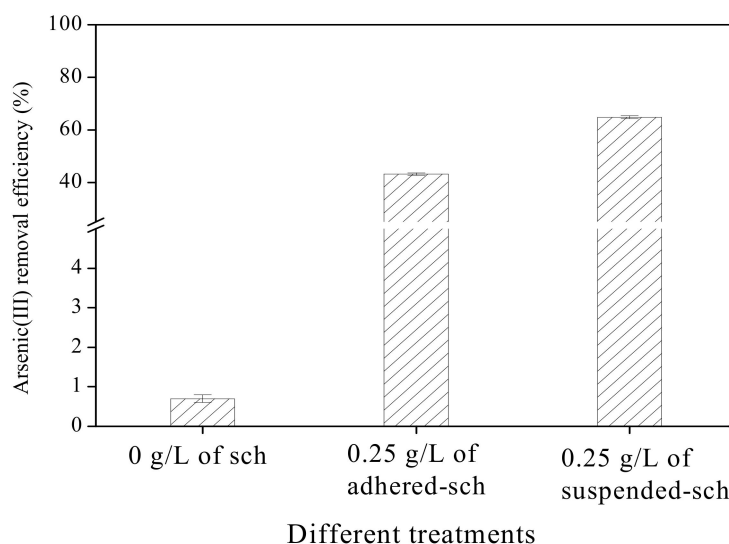


**Figure 7.** Arsenic(III) removal efficiency by schwertmannite adhered to the flask wall during bio-synthesis (adhered-sch) and by schwertmannite suspended in the liquid during bio-synthesis (suspended-sch).

In contrast, when 0.25 g/L of either adhered-sch or suspended-sch were added and adsorbed arsenic(III) under 28 °C and 160 rpm, the arsenic(III) removal efficiency sharply increased at 4 h. For water with an initial 1 mg/L arsenic(III) concentration at pH 7.5, the addition of 0.25 g/L adhered-sch as an adsorbent resulted in an arsenic(III) removal efficiency of 43.2% after 4 h adsorption. However, the arsenic(III) removal efficiency could be increased by 50% over the same adsorption period by adding 0.25 g/L suspended-sch as the adsorbent. Liao et al. [21] observed that the arsenic(III) removal efficiency can reach 99.1% at 4 h under 25 °C and 180 rpm reaction conditions with the addition of 0.25 g/L bio-schwertmannite as the adsorbent in a similar arsenic(III)-bearing solution system. It is indicated that the arsenic(III) removal efficiency has a close relationship with the reaction conditions, which will be focused on in a further study.

## 4. Conclusions

During schwertmannite bio-synthesis by *A. ferrooxidans* LX5, some of the synthesized schwertmannite adheres to the reactor wall (designated as adhered-sch), while the rest remains suspended in the system (designated as suspended-sch). The morphology of adhered-sch and suspended-sch differs significantly, with the former consisting of relatively large spheres having fractured surfaces and the latter exhibiting a relatively less compact spiny structure reminiscent of a hedgehog. Consequently, the total pore volume, specific surface area, and arsenic(III) removal efficiency of adhered-sch are smaller than for the suspended-sch. In both adhered-sch and suspended-sch, mesopores in the synthesized schwertmannite represent a modest pore volume (~30% of total pore volume), but make a great contribution to the specific surface area (~65% of total specific surface area); this relationship is especially true for mesopores with a ~3–20 nm diameter. Additional schwertmannite introduced into a bio-synthesis systems can reduce the amount of adhered-sch due to the friction effect between the introduced schwertmannite and the reactor wall. The addition

of 13.3–26.7 g/L of schwertmannite can eliminate schwertmannite adherence on the reactor wall and improve the ferrous ion efficiency to a certain extent. However, ferrous ion bio-oxidation can be inhibited when the amount of introduced schwertmannite exceeds some threshold (in this study, when the added schwertmannite increased from 13.3 g/L to 26.7 g/L). The outcomes of this study provide the necessary data for schwertmannite bio-synthesis and provide a scientific basis for enhancing arsenic(III) removal from arsenic(III)-bearing groundwater. In a word, some additional schwertmannite introduced into a schwertmannite bio-synthesis systems before ferrous ion bio-oxidation can increase the suspended-sch harvested quantity when ferrous ions completely bio-oxidized. Effective bio-synthesis of suspended-sch is more beneficial to the removal of arsenic(III) from arsenic(III)-bearing groundwater in practical application.

**Acknowledgments:** This work was supported by the National Natural Science Foundation of China (21637003, 21407102), the Natural Science Foundation of Shanxi Province, China (2015011022), and the Program for the Top Young Innovative Talents of Shanxi Agricultural University (TYIT 201405).

**Author Contributions:** J.Z., L.Z. and F.L. conceived and designed the experiments; J.Z., S.Z. and J.X. performed the experiments; J.Z. and S.Z. analyzed the data; J.S., Y.G. and W.F. contributed reagents/materials/analysis tools; and J.Z. and S.Z. wrote the paper.

**Conflicts of Interest:** The authors declare no conflict of interest.

## References

1. Podder, M.S.; Majumder, C.B. Phycoremediation of arsenic from wastewaters by *Chlorella pyrenoidosa*. *Groundw. Sustain. Dev.* **2015**, *1*, 8–91. [[CrossRef](#)]
2. Podder, M.S.; Majumder, C.B. Study of the kinetics of arsenic removal from wastewater using *Bacillus arsenicus* biofilms supported on a Neem leaves/MnFe<sub>2</sub>O<sub>4</sub> composite. *Ecol. Eng.* **2016**, *88*, 195–216. [[CrossRef](#)]
3. Smedley, P.L.; Kinniburgh, D.G. A review of the source, behaviour and distribution of arsenic in natural waters. *Appl. Geochem.* **2002**, *17*, 517–568. [[CrossRef](#)]
4. Li, H.; Zeng, X.C.; He, Z.; Chen, X.; Guoji, E.; Han, Y.; Wang, Y. Long-term performance of rapid oxidation of arsenite in simulated groundwater using a population of arsenite-oxidizing microorganisms in a bioreactor. *Water Res.* **2016**, *101*, 393–401. [[CrossRef](#)] [[PubMed](#)]
5. Kanel, S.R.; Manning, B.; Charlet, L.; Choi, H. Removal of arsenic(III) from groundwater by nanoscale zero-valent iron. *Environ. Sci. Technol.* **2005**, *39*, 1291–1298. [[CrossRef](#)] [[PubMed](#)]
6. Li, Z.; Halem, D.V.; Verberk, J. Review of high arsenic groundwater in China. In Proceedings of the 4th International Conference on Bioinformatics & Biomedical Engineering, Chengdu, China, 18–20 June 2010; pp. 1–4.
7. He, J.; Ma, T.; Deng, Y.; Yang, H.; Wang, Y. Environmental geochemistry of high arsenic groundwater at western Hetao plain, Inner Mongolia. *Front. Earth Sci.* **2009**, *3*, 63–72. [[CrossRef](#)]
8. Xie, X.J.; Ellis, A.; Wang, Y.; Xie, Z.; Duan, M.; Su, C. Geochemistry of redox-sensitive elements and sulfur isotopes in the high arsenic groundwater system of Datong Basin, China. *Sci. Total Environ.* **2009**, *407*, 3823–3835. [[CrossRef](#)] [[PubMed](#)]
9. Liu, F.F.; Wang, J.P.; Zheng, Y.J.; Ng, J.C. Biomarkers for the evaluation of population health status 16 years after the intervention of arsenic-contaminated groundwater in Xinjiang, China. *J. Hazard. Mater.* **2013**, *262*, 1159–1166. [[CrossRef](#)] [[PubMed](#)]
10. Ahamed, S.; Sengupta, M.K.; Mukherjee, A.; Hossain, M.A.; Das, B.; Nayak, B.; Pal, A.; Mukherjee, S.C.; Pati, S.; Dutta, R.N. Arsenic groundwater contamination and its health effects in the state of Uttar Pradesh (UP) in upper and middle Ganga plain, India: A severe danger. *Sci. Total Environ.* **2006**, *370*, 310–322. [[CrossRef](#)] [[PubMed](#)]
11. Karim, M.M. Arsenic in groundwater and health problems in Bangladesh. *Water Res.* **2000**, *34*, 304–310. [[CrossRef](#)]
12. Zhao, D.D.; Yang, Y.; Chen, J.P. Zirconium/polyvinyl alcohol modified flat-sheet polyvinylidene fluoride membrane for decontamination of arsenic: Material design and optimization, study of mechanisms, and application prospects. *Chemosphere* **2016**, *155*, 630–639. [[CrossRef](#)] [[PubMed](#)]

13. Pessoa-Lope, M.; Crespo, J.G.; Velizarov, S. Arsenate removal from sulphate-containing water streams by an ion-exchange membrane process. *Sep. Purif. Technol.* **2016**, *166*, 125–134. [[CrossRef](#)]
14. Ali, I.; Khan, T.A.; Asim, M. Removal of arsenic from water by electrocoagulation and electro dialysis techniques. *Sep. Purif. Rev.* **2011**, *40*, 25–42. [[CrossRef](#)]
15. Peng, B.; Song, T.T.; Wang, T.; Chai, L.; Yang, W.; Li, X.; Li, C.; Wang, H. Facile synthesis of Fe<sub>3</sub>O<sub>4</sub>@Cu(OH)<sub>2</sub> composites and their arsenic adsorption application. *Chem. Eng. J.* **2016**, *299*, 15–22. [[CrossRef](#)]
16. Kumar, A.S.K.; Jiang, S.J. Chitosan-functionalized graphene oxide: A novel adsorbent an efficient adsorption of arsenic from aqueous solution. *J. Environ. Chem. Eng.* **2016**, *4*, 1698–1713. [[CrossRef](#)]
17. Kofa, G.P.; Ndikoungou, S.; Kayem, G.J.; Kamga, R. Adsorption of arsenic by natural pozzolan in a fixed bed: Determination of operating conditions and modeling. *J. Water Process Eng.* **2015**, *6*, 166–173. [[CrossRef](#)]
18. Dou, X.M.; Mohan, D.; Pittman, C.U., Jr. Arsenate adsorption on three types of granular schwertmannite. *Water Res.* **2013**, *47*, 2938–2948. [[CrossRef](#)] [[PubMed](#)]
19. Dey, A.; Singh, R.; Purkait, M.K. Cobalt ferrite nanoparticles aggregated schwertmannite: A novel adsorbent for the efficient removal of arsenic. *J. Water Process Eng.* **2014**, *3*, 1–9. [[CrossRef](#)]
20. Liu, F.W.; Zhou, J.; Zhang, S.S.; Liu, L.; Zhou, L.; Fan, W. Schwertmannite synthesis through ferrous ion chemical oxidation under different H<sub>2</sub>O<sub>2</sub> supply rates and its removal efficiency for arsenic from contaminated groundwater. *PLoS ONE* **2015**, *10*, e0138891. [[CrossRef](#)] [[PubMed](#)]
21. Liao, Y.H.; Liang, J.R.; Zhou, L.X. Adsorptive removal of As(III) by biogenic schwertmannite from simulated As-contaminated groundwater. *Chemosphere* **2011**, *83*, 295–301. [[CrossRef](#)] [[PubMed](#)]
22. Mokadem, N.; Demdoum, A.; Hamed, Y.; Bouri, S.; Hadji, R.; Boyce, A.; Laouar, R.; Saad, A. Hydrogeochemical and stable isotope data of groundwater of a multi-aquifer system: Northern Gafsa basin—Central Tunisia. *J. Afr. Earth Sci.* **2016**, *114*, 174–191. [[CrossRef](#)]
23. Li, X.Q.; Hou, X.W.; Zhou, Z.C.; Liu, L.X. Geochemical provenance and spatial distribution of fluoride in groundwater of Taiyuan basin, China. *Environ. Earth. Sci.* **2011**, *62*, 1635–1642. [[CrossRef](#)]
24. Paikaray, S.; Göttlicher, J.; Peiffer, S. Removal of As(III) from acidic waters using schwertmannite: Surface speciation and effect of synthesis pathway. *Chem. Geol.* **2011**, *283*, 134–142. [[CrossRef](#)]
25. Qiao, X.X.; Liu, L.L.; Shi, J.; Zhou, L.X.; Guo, Y.H.; Ge, Y.Y.; Fan, W.H.; Liu, F.W. Heating changes bio-schwertmannite microstructure and arsenic(III) removal efficiency. *Minerals* **2017**, *7*, 9. [[CrossRef](#)]
26. Xu, Y.Q.; Yang, M.; Yao, T.; Xiong, H. Isolation, identification and arsenic-resistance of *Acidithiobacillus ferrooxidans* HX3 producing schwertmannite. *J. Environ. Sci.* **2014**, *26*, 1463–1470. [[CrossRef](#)] [[PubMed](#)]
27. Liu, F.W.; Zhou, J.; Zhou, L.X.; Zhang, S.S.; Liu, L.L.; Wang, M. Effect of neutralized solid waste generated in lime neutralization on the ferrous ion bio-oxidation process during acid mine drainage treatment. *J. Hazard. Mater.* **2015**, *299*, 404–411. [[CrossRef](#)] [[PubMed](#)]
28. Liao, Y.H.; Zhou, L.X.; Liang, J.R.; Xiong, H.X. Biosynthesis of schwertmannite by *Acidithiobacillus ferrooxidans* cell suspensions under different pH condition. *Mater. Sci. Eng. C* **2009**, *29*, 211–215. [[CrossRef](#)]
29. Liu, F.W.; Zhou, J.; Jing, T.J.; Zhang, S.S.; Liu, L.L. Effect of calcium oxide on the efficiency of ferrous ion oxidation and total iron precipitation during ferrous ion oxidation in simulated acid mine drainage treatment with inoculation of *Acidithiobacillus ferrooxidans*. *Water Sci. Technol.* **2016**, *73*, 1442–1452. [[CrossRef](#)] [[PubMed](#)]
30. Zhang, J.; Zhao, Y.B.; Zhao, X.; Liu, Z.L.; Chen, W. Porous perovskite LaNiO<sub>3</sub> nanocubes as cathode catalysts for Li-O<sub>2</sub> batteries with Low charge potential. *Sci. Rep.* **2014**, *4*, 6005. [[CrossRef](#)] [[PubMed](#)]
31. Huo, J.; Aguilerasigalat, J.; Elhankari, S.; Bradshaw, D. Magnetic MOF microreactors for recyclable size-selective biocatalysis. *Chem. Sci.* **2014**, *6*, 1938–1943. [[CrossRef](#)]
32. Bian, C.; Ji, L.Y.; Liu, P. Determination of As and Hg Simultaneously in Wheat Flour by Dual Channel Atomic Fluorescence Spectrometry. *J. Chin. Cereals Oils Assoc.* **2013**, *28*, 108–111.
33. Joint Committee on Powder Diffraction Standards (JCPDS). *Mineral Powder Diffraction Files*; International Center for Diffraction Data: Swarthmore, PA, USA, 2002.
34. Veríssimo, L.M.P.; Ribeiro, A.C.F.; Lobo, V.M.M.; Esteso, M.A. Effect of hydrolysis on the diffusion of ferric sulphate in aqueous solutions at T = 298.15 K. *J. Chem. Thermodyn.* **2012**, *55*, 56–59. [[CrossRef](#)]
35. Wang, M.; Zhou, L.X. Simultaneous oxidation and precipitation of iron using jarosite immobilized *Acidithiobacillus ferrooxidans* and its relevance to acid mine drainage. *Hydrometallurgy* **2012**, *125–126*, 152–156. [[CrossRef](#)]
36. Liu, J.Y.; Tao, X.X.; Cai, P. Study of formation of jarosite mediated by *thiobacillus ferrooxidans* in 9K medium. *Procedia Earth Planet. Sci.* **2009**, *1*, 706–712. [[CrossRef](#)]

37. Su, G.Z.; Lu, J.J.; Lu, X.C.; Li, J.; Tu, B.W. An experimental study of the adsorption of  $\text{Cu}^{2+}$  and *Acidithiobacillus ferrooxidans* on schwertmannite. *Acta Petrol. Mineral.* **2009**, *28*, 575–580.
38. Wang, K.B.; Fang, D.; Xu, Z.H.; Shi, Y.; Zheng, G.Y.; Zhou, L.X. Biosynthetic schwertmannite as catalyst in Fenton-like reactions for degradation of methyl orange. *Environ. Sci.* **2015**, *36*, 995–999.
39. Bigham, J.M.; Schwertmann, U.; Carlson, L.; Murad, E. A poorly crystallized oxyhydroxysulfate of iron formed by bacterial oxidation of Fe(II) in acid mine waters. *Geochim. Cosmochim. Acta* **1990**, *54*, 2743–2758. [[CrossRef](#)]
40. Oseto, K.; Okabe, H.; Okatsu, K. Evaluation of waterflooding performance utilizing core analysis data for carbonate reservoir, offshore Abu Dhabi. *J. Jpn. Assoc. Pet. Technol.* **2007**, *72*, 594–600. [[CrossRef](#)]
41. Lee, D.; Jung, J.Y.; Jung, M.J.; Lee, Y.S. Hierarchical porous carbon fibers prepared using a  $\text{SiO}_2$  template for high-performance EDLCs. *Chem. Eng. J.* **2015**, *263*, 62–70. [[CrossRef](#)]
42. Peng, J.H.; Zhang, L.B.; Zhang, S.M.; Tu, J.H.; Xia, H.Y.; Fan, X.X.; Guo, S.H. Study on Preparation of Micropore Activated Carbons from Tobacco Stems Impregnated with Zinc Chloride by Microwave Heating. *J. Mater. Sci. Eng.* **2006**, *24*, 52–57.
43. Hsieh, C.T.; Teng, H. Influence of mesopore volume and adsorbate size on adsorption capacities of activated carbons in aqueous solutions. *Carbon* **2000**, *38*, 863–869. [[CrossRef](#)]



© 2017 by the authors. Licensee MDPI, Basel, Switzerland. This article is an open access article distributed under the terms and conditions of the Creative Commons Attribution (CC BY) license (<http://creativecommons.org/licenses/by/4.0/>).